LETTER

doi:10.1038/nature19075

Emergence of a *Homo sapiens*-specific gene family and chromosome 16p11.2 CNV susceptibility

Xander Nuttle[1]*, Giuliana Giannuzzi[2]*, Michael H. Duyzend[1], Joshua G. Schraiber[1], Iñigo Narvaiza[3], Peter H. Sudmant[1]†, Osnat Penn[1], Giorgia Chiatante[4], Maika Malig[1], John Huddleston[1,5], Chris Benner[3], Francesca Camponeschi[6], Simone Ciofi-Baffoni[6,7], Holly A. F. Stessman[1], Maria C. N. Marchetto[3], Laura Denman[1], Lana Harshman[1], Carl Baker[1], Archana Raja[1,5], Kelsi Penewit[1], Nicolette Janke[1], W. Joyce Tang[8], Mario Ventura[4], Lucia Banci[6,7], Francesca Antonacci[4], Joshua M. Akey[1], Chris T. Amemiya[8], Fred H. Gage[3,9], Alexandre Reymond[2] & Evan E. Eichler[1,5]

Genetic differences that specify unique aspects of human evolution have typically been identified by comparative analyses between the genomes of humans and closely related primates[1], including more recently the genomes of archaic hominins[2,3]. Not all regions of the genome, however, are equally amenable to such study. Recurrent copy number variation (CNV) at chromosome 16p11.2 accounts for approximately 1% of cases of autism[4,5] and is mediated by a complex set of segmental duplications, many of which arose recently during human evolution. Here we reconstruct the evolutionary history of the locus and identify bolA family member 2 (*BOLA2*) as a gene duplicated exclusively in *Homo sapiens*. We estimate that a 95-kilobase-pair segment containing *BOLA2* duplicated across the critical region approximately 282 thousand years ago (ka), one of the latest among a series of genomic changes that dramatically restructured the locus during hominid evolution. All humans examined carried one or more copies of the duplication, which nearly fixed early in the human lineage—a pattern unlikely to have arisen so rapidly in the absence of selection ($P < 0.0097$). We show that the duplication of *BOLA2* led to a novel, human-specific in-frame fusion transcript and that *BOLA2* copy number correlates with both RNA expression ($r = 0.36$) and protein level ($r = 0.65$), with the greatest expression difference between human and chimpanzee in experimentally derived stem cells. Analyses of 152 patients carrying a chromosome 16p11.2 rearrangement show that more than 96% of breakpoints occur within the *H. sapiens*-specific duplication. In summary, the duplicative transposition of *BOLA2* at the root of the *H. sapiens* lineage about 282 ka simultaneously increased copy number of a gene associated with iron homeostasis and predisposed our species to recurrent rearrangements associated with disease.

To reconstruct the evolutionary history of the chromosome 16p11.2 region, we generated complete, reference-quality genome sequences[6] (Supplementary Table 1) for one orangutan, two chimpanzee and three human haplotypes (Fig. 1a and Extended Data Fig. 1). Comparison with mouse establishes the orangutan configuration as ancestral. In both humans and chimpanzees, the region has been independently restructured, nearly doubling in length primarily by the differential accumulation of segmental duplications (Fig. 1a and Extended Data Fig. 1a). We find six inversions have occurred in the African great apes within chromosome 16p11.2 (Extended Data Figs 2–4 and Supplementary Tables 2 and 3), a nonrandom clustering ($P < 1 \times 10^{-6}$), with breakpoints mapping near an ~20-kilobase-pair (kbp) low-copy repeat 16a (LCR16a) core duplicon. The core encodes a positively selected gene family (*NPIP*) that emerged on the human–African great ape lineage[7]. Only within the human lineage do large (>100 kbp) segmental duplications exist in a direct orientation flanking the autism critical region at breakpoint regions BP4 and BP5 (Extended Data Fig. 5a and Supplementary Table 4)[8], implying that susceptibility to large-scale CNV associated with disease[4,5,9] arose specifically within the human species.

Structural differences between human haplotypes are largely restricted to integral changes in the copy number of a 102-kbp block within both the proximal and distal breakpoint regions (Extended Data Fig. 1b). This block is composed of two different segmental duplications originating from chromosome 16: a 72-kbp segment duplicated from chromosome 16p12.1 carrying *NPIP* and a portion of the *SMG1* serine–threonine kinase gene (*SMG1P*) and a 30-kbp segment carrying three intact genes: *BOLA2*, *SLX1* and *SULT1A3* (Fig. 1a and Extended Data Fig. 1b). More than a dozen large-scale structural changes, including six duplicative transpositions (>830 kbp) from elsewhere on chromosome 16, are required to reconcile the organization of human and chimpanzee chromosome 16p11.2 (Extended Data Figs 3, 4 and Supplementary Table 3). Assuming a human–chimpanzee divergence time of 6 million years ago (Ma) (ref. 10) and a constant substitution rate, we estimate that a 95-kbp segment including *BOLA2* duplicated across the critical region ~282 ka (95% confidence interval 361–209 ka), around the time when *H. sapiens* emerged as a species[11] (Figs 1b and 2a, Extended Data Fig. 6 and Supplementary Tables 5–7).

We examined copy number diversity[12] of the duplicated genes mapping to the 102-kbp cassette—*BOLA2*, *SLX1* and *SULT1A3*—in humans, archaic humans and apes (Fig. 2b–c, Extended Data Fig. 7 and Supplementary Tables 8–10). We found that *BOLA2* is duplicated in all *H. sapiens* individuals examined, including archaic representatives of Neolithic and Mesolithic populations[13], as well as the oldest sequenced archaic human, Ust'-Ishim, estimated to have lived 45 ka (ref. 14). In sharp contrast, *BOLA2* is single copy (that is, diploid copy number = 2) in nonhuman primates and the archaic hominins Neanderthal[2] and Denisova[3] (Fig. 2b–c and Supplementary Table 8), consistent with our phylogenetic point estimate of the duplication age. Human genomes contain from three to eight diploid *BOLA2* copies, with at least one copy of the distal duplicate *BOLA2B* (range one to four copies; mean and median two) and at least two copies of the proximal ancestral *BOLA2A* (range two to five copies; mean and median four; Fig. 2c and Supplementary Table 8).

[1]Department of Genome Sciences, University of Washington School of Medicine, Seattle, Washington 98195, USA. [2]Center for Integrative Genomics, University of Lausanne, 1015 Lausanne, Switzerland. [3]Laboratory of Genetics, The Salk Institute for Biological Studies, 10010 North Torrey Pines Road, La Jolla, California 92037, USA. [4]Dipartimento di Biologia, Università degli Studi di Bari 'Aldo Moro', Bari 70125, Italy. [5]Howard Hughes Medical Institute, Seattle, Washington 98195, USA. [6]Department of Chemistry, University of Florence, Via della Lastruccia 3, 50019 Sesto Fiorentino, Florence, Italy. [7]Magnetic Resonance Center CERM, University of Florence, Via Luigi Sacconi 6, 50019, Sesto Fiorentino, Florence, Italy. [8]Benaroya Research Institute at Virginia Mason, Seattle, Washington 98101, USA. [9]Center for Academic Research and Training in Anthropogeny (CARTA), 9500 Gilman Drive, La Jolla, California 92093, USA. †Present address: Program in Computational and Systems Biology, Massachusetts Institute of Technology, Cambridge, Massachusetts 02142, USA.
*These authors contributed equally to this work.

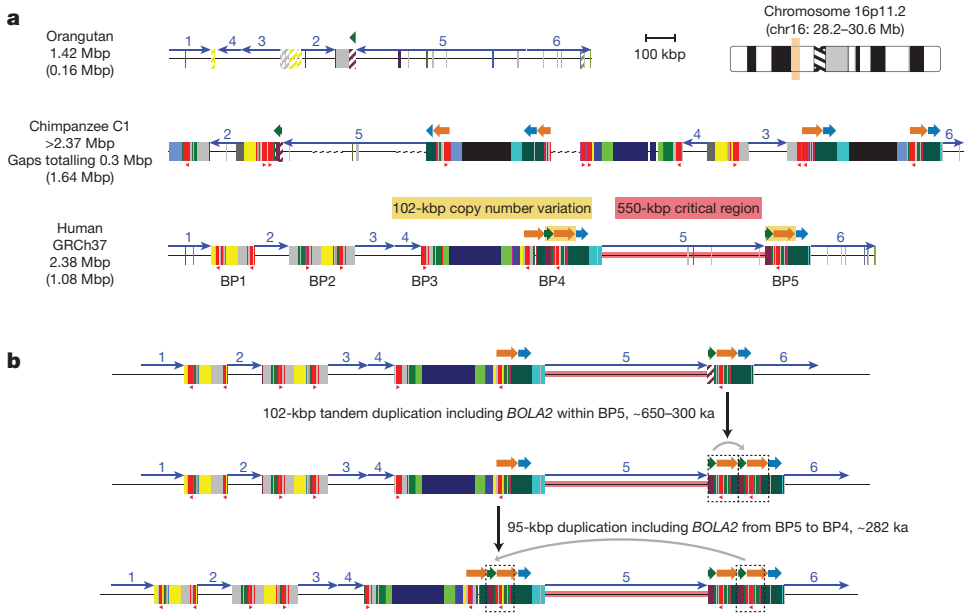

Figure 1 | Comparative sequence analysis of chromosome 16p11.2 among apes and the evolution of *BOLA2* duplications in humans. **a**, Genomic organization of chromosome 16p11.2 for one orangutan and one chimpanzee haplotype and the human reference haplotype (GRCh37 chr16:28195661–30573128). Blocks of segmental duplications within this locus mediate recurrent rearrangements in humans and have thus been defined as breakpoint regions BP1–BP5 (ref. 8). Coloured boxes and thick arrows indicate the extent and orientation of segmental duplications (different colours denote duplicons from different ancestral genomic loci; hashed boxes indicate sequence duplicated in humans but not in the species represented). Thin numbered arrows show orientations of gene-rich regions of unique sequence. Red triangles indicate locations and orientations of *NPIP* cores. Numbers (left) indicate the size of each haplotype, with the number of segmentally duplicated base pairs shown in parentheses. For chimpanzee, the size is a lower bound owing to gaps (dotted line sections) and the contig not reaching unique region 1. Regions of human CNV (yellow highlight) occur on both sides of the critical region and involve the same 102-kbp unit: a 30-kbp block (green arrow) containing *BOLA2*, *SLX1* and *SULT1A3* and a 72-kbp block (orange arrow) harbouring *SMG1P*. Expansion and contraction of this cassette underlie hundreds of kilobase pairs of structural diversity between human haplotypes. **b**, A model for the emergence of *BOLA2* duplications during *H. sapiens* evolution. It depicts structural changes over time leading to the present-day human architecture. A full evolutionary model detailing the dynamic evolution of chromosome 16p11.2 in great apes is provided in the Supplementary Information and Extended Data Figs 3 and 4.

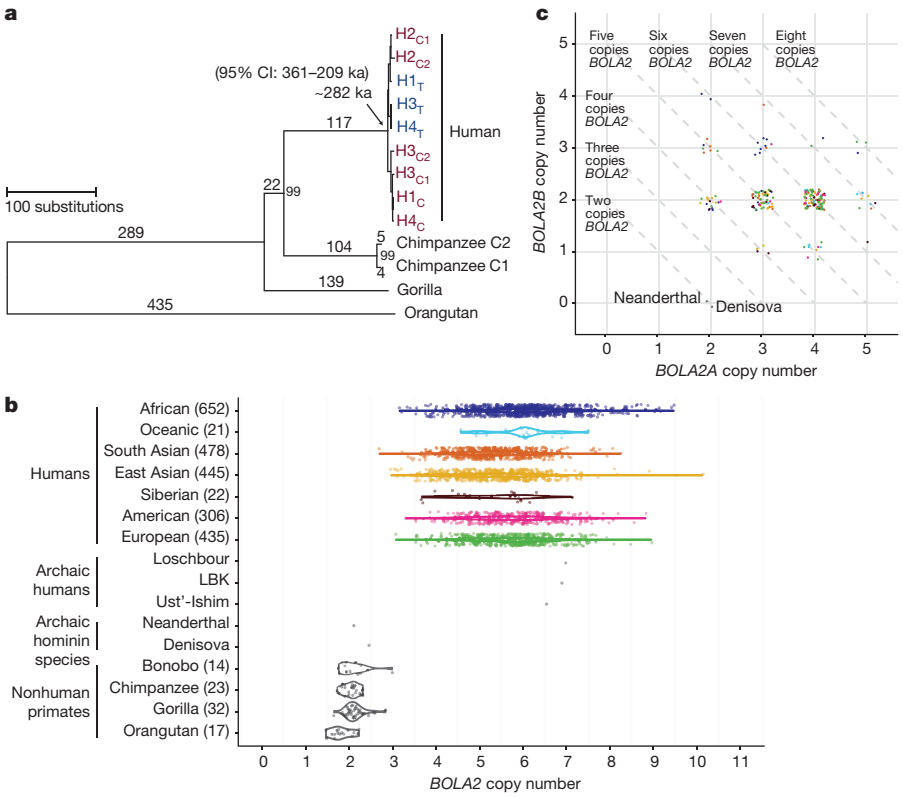

Figure 2 | *H. sapiens*-specific *BOLA2* duplication and copy number diversity. **a**, A phylogenetic tree representing the last interspersed segmental duplication from BP5 to BP4 in humans. The unrooted neighbour-joining tree was constructed from a 21,102-bp multiple sequence alignment including allelic, paralogous and orthologous copies of the *BOLA2*-containing segmental duplications. Human taxon labels denote haplotypes and locations of different copies (telomeric, T, blue; centromeric, C, red, with C1 closer to the critical region than C2). The number of substitutions (above each branch) and bootstrap support (at nodes) are indicated. Timing estimates assume human–chimpanzee divergence 6 Ma (ref. 10). **b**, Diploid copy number estimates (points) for *BOLA2* based on sequence read depth[12] are shown for 2,359 humans, three archaic humans[13,14], a Neanderthal[2], a Denisovan[3] and 86 nonhuman primates, with violin plots overlaid. **c**, Paralogue-specific *BOLA2* copy number genotypes (points, jittered around their integer values) were inferred from WGS read depth over informative markers for 222 individuals sequenced to high coverage. Colours correspond to different populations as in **b**.

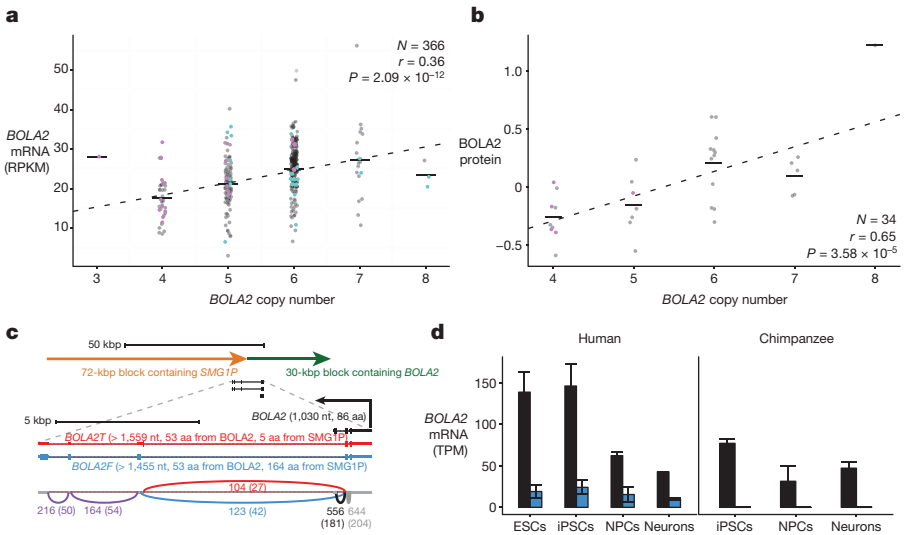

Figure 3 | *BOLA2* expression analyses. a, *BOLA2* mRNA expression quantifications[20] in 366 LCLs from individuals genotyped for *BOLA2* paralogue-specific copy number. Points indicate expression levels and copy number (jittered) for each cell line; horizontal lines show mean levels for each copy number. Dashed line shows least squares regression. Point colours indicate *BOLA2B* copy number (pink, one copy; black, two copies; cyan, three copies). Groups with the same aggregate *BOLA2* copy number but different combinations of paralogue-specific copy number do not exhibit differential expression, consistent with both paralogues producing mRNA. RPKM, reads per kilobase of transcript per million mapped reads. **b**, Plot layout as in **a**, but data show BOLA2 protein expression quantified by western blot densitometry on protein lysates from 34 LCLs. No evidence indicates differential protein expression of distinct *BOLA2* paralogues. **c**, *BOLA2* gene models, predicted protein products and support from RNA-seq data from human iPSCs. RT–PCR, cloning and capillary sequencing experiments identified three *BOLA2* isoforms: the canonical isoform (*BOLA2*, black) and two fusion isoforms consisting of the first two exons from canonical *BOLA2* fused with three exons from *SMG1P*. One fusion isoform (*BOLA2F*, blue) maintains the *BOLA2* open reading frame well beyond the fusion junction, whereas a third isoform (*BOLA2T*, red) contains a premature stop codon within the first *SMG1P*-derived exon. Numbers next to curved lines indicate mean counts of RNA-seq reads from two human iPSCs (two independent clones each) supporting each exon–exon junction, with standard errors in parentheses. nt, nucleotides; aa, amino acids. **d**, RNA-seq quantification of *BOLA2* (black) and *BOLA2F* (blue) mRNA expression through *in vitro* differentiation of primate iPSCs into neurons. Data from two human and two chimpanzee cell lines (two independent clones each, except for neurons) reveal higher levels of *BOLA2* transcripts in human iPSCs than in chimpanzee iPSCs and that *BOLA2* RNA levels decrease through neuronal differentiation. Bar heights indicate mean expression levels for each species and differentiation stage in transcripts per million (TPM); error bars, s.e.m. *BOLA2* expression in human embryonic stem cells (two cell lines) is consistent with data from human iPSCs. ESCs, embryonic stem cells; NPCs, neural progenitor cells.

In light of its recent origin and its potential to promote disease-causing rearrangement, we considered it remarkable that 99.8% of humans carry four or more copies of this segment. Ancient humans such as Ust'-Ishim as well as some of the oldest branches of modern humans (for example, San and Biaka pygmy[15]) typically carry five or six copies, indicating that it spread rapidly early in human history. We modelled various evolutionary scenarios by simulation on the basis of the observed genotypes and a realistic model of human demographic history (Extended Data Fig. 8a), assuming neutral evolution[16–18]. The observed genotypes or genotypes with higher *BOLA2B* frequencies only in humans were improbable ($P < 0.0097$; Extended Data Fig. 8b), even when the duplication age parameter was varied by an order of magnitude. Scenarios incorporating recurrent duplication were also deemed unlikely ($P < 0.0062$). We next implemented a model incorporating the 282 ka age estimate but varying the selection coefficient (s) as an input parameter, yielding a maximum likelihood estimate of $s = 0.0015$ (Extended Data Fig. 8c). Interestingly, the unique ~550-kbp critical region flanked by *BOLA2* duplications showed signatures consistent with a region under positive selection: the absence of archaic introgression[19], low diversity (bottom 2.7%) and an excess of rare variants (Extended Data Fig. 8d–e).

Because humans show extensive CNV, we assessed whether copy number correlated with messenger RNA (mRNA) and protein levels. We found a significant correlation between *BOLA2* copy number and expression at the RNA level from analysis of 366 lymphoblastoid cell lines (LCLs)[20] ($r = 0.36$, $P = 2.09 \times 10^{-12}$; Fig. 3a and Supplementary Tables 11 and 12) and at the protein level from analysis of whole-protein lysates from 34 LCLs ($r = 0.64$, $P = 4.34 \times 10^{-5}$; Fig. 3b and Supplementary Tables 13 and 14).

We also performed reverse transcription PCR (RT–PCR) and identified an alternative gene structure composed of the first two exons from *BOLA2* joined with three novel 3′ exons from an older segmental duplication containing *SMG1P* (Fig. 3c). This fusion isoform contains an open reading frame predicted to encode a 217-residue protein, including 53 residues from BOLA2 and 164 residues from SMG1P. Both canonical and fusion transcripts are co-expressed in a wide variety of tissues and developmental stages (Extended Data Fig. 9). Although the predicted fusion protein cannot be detected by existing antibodies, it is interesting that ribosome profiling data provide evidence that the mRNA is translated (Supplementary Table 15). Importantly, since the ancestral *BOLA2* at BP5 lacked the *SMG1P* duplication downstream, the origin of the fusion product must have coincided with the juxtaposition of *BOLA2* and *SMG1P* by the tandem 102-kbp segmental duplication ~650–300 ka at BP5. We conclude that this fusion isoform is *H. sapiens*-specific.

BOLA2 was previously identified as one of the top 50 genes differentially expressed between humans and nonhuman apes in induced pluripotent stem cells (iPSCs)[21], implying that this gene might be particularly relevant early in development. On the basis of our characterization of the different *BOLA2* isoforms, we revisited this observation by quantifying *BOLA2* mRNA levels by RNA sequencing (RNA-seq) in human and chimpanzee iPSCs, iPSC-derived neural progenitor cells and 8-week-old neurons. Remarkably, we found the greatest differences in canonical *BOLA2* expression at the iPSC state (twofold) and to a lesser extent in neural progenitor cells (1.5-fold) (Fig. 3d and Supplementary Table 16). Quantification of *BOLA2* expression in two primary human embryonic stem cell lines revealed transcript levels comparable to human iPSCs (Fig. 3d and Supplementary Table 16).

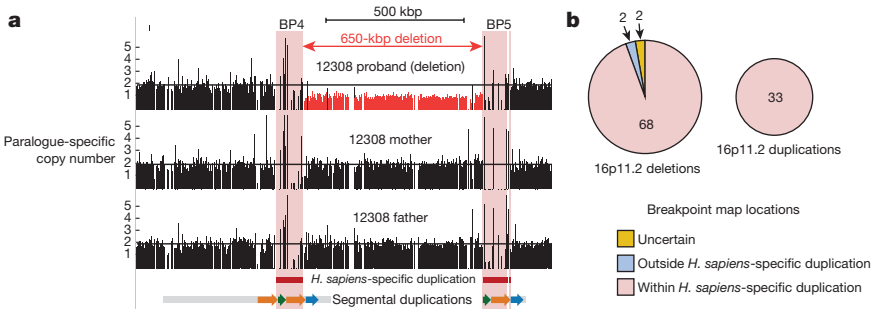

Figure 4 | Refinement of chromosome 16p11.2 rearrangement breakpoints. a, WGS results for a family with a *de novo* chromosome 16p11.2 microdeletion in a child with autism. Normalized read depth at unique 30-mer positions in the human reference genome GRCh37 is depicted for the proband, her mother and her father. Read-depth signatures reveal a deletion in the proband extending between but not beyond the *H. sapiens*-specific duplicated sequences (highlighted in pink). **b**, Summary of results across 105 independent microdeletion and microduplication events from 152 individuals; ~96% of breakpoints map to the *H. sapiens*-specific segmental duplication.

In contrast, examination of a panel of adult tissues[22] revealed no substantial differences in *BOLA2* mRNA levels between human and chimpanzee (Extended Data Fig. 9d). As expected, expression of the fusion *BOLA2–SMG1P* transcript was detected exclusively in human.

The duplication of *BOLA2* across the critical region expanded threefold the size of flanking high-identity, directly oriented sequence blocks (Extended Data Fig. 5a–b and Supplementary Tables 4, 17 and 18), theoretically predisposing the locus to recurrent CNV via unequal crossover (Extended Data Fig. 5c) specifically in the human lineage. To test this, we refined breakpoint locations in patients with autism and developmental delay carrying either the chromosome 16p11.2 microduplication or microdeletion event[23]. Using whole-genome sequence (WGS) data and a molecular inversion probe (MIP) assay[24], we localized breakpoints in 152 patients corresponding to 105 independent rearrangement events (Fig. 4a, Extended Data Fig. 10 and Supplementary Table 19). We found 96% (101 out of 105) of the disease-causing rearrangement breakpoints map within the *H. sapiens*-specific duplication containing *BOLA2* (Fig. 4b). Thus, the expansion of this segment rendered the chromosome 16p11.2 locus susceptible to recurrent rearrangement.

In summary, the level of genetic difference between humans and chimpanzees for chromosome 16p11.2 stands in sharp contrast to the oft-quoted 99% genetic identity between the species. The region has undergone extensive inversion and duplication, including a 95-kbp segment containing *BOLA2* that duplicated after our divergence with ancient hominins. This event contributes more derived sequence specific to *H. sapiens* than 35,500 previously reported human-specific single-nucleotide variants and indels combined[2]. The rapid rise and dispersal of this duplicated segment at the root of *H. sapiens* (~282 ka) are unlikely to have occurred under neutral evolution but rather are consistent with modest positive selection ($s = 0.0015$). The estimated strength of selection on the *BOLA2* duplication is an order of magnitude weaker than what is typically observed for recent positive selection (such as the emergence of lactase persistence ~10 ka (ref. 25)) but an order of magnitude stronger than nearly neutral mutations. Remarkably, the *BOLA2* duplication rapidly rose to high frequency in humans despite predisposing our species to recurrent CNV associated with disease. The expansion of this segment resulted in the formation of a novel fusion transcript and dramatic *BOLA2* expression differences between chimpanzee and human iPSCs. Although the phenotypic consequences of increased BOLA2 expression and the novel fusion transcript await future *in vivo* characterization, it is known that BOLA2 physically interacts in a heterotrimeric complex with GLRX3 (glutaredoxin 3)[26]. This complex is conserved from prokaryotes to humans[27] and was shown to have a role in iron sensing in yeast[28]. In vertebrates, BOLA2 has been hypothesized to play important roles in iron regulation[29] and iron–sulfur protein biogenesis[30]. We speculate that the expansion of this conserved gene may enhance iron utilization and homeostasis, especially during human embryonic development.

Online Content Methods, along with any additional Extended Data display items and Source Data, are available in the online version of the paper; references unique to these sections appear only in the online paper.

Received 29 October 2015; accepted 2 July 2016.
Published online 3 August 2016.

1. King, M. C. & Wilson, A. C. Evolution at two levels in humans and chimpanzees. *Science* **188,** 107–116 (1975).
2. Prüfer, K. *et al.* The complete genome sequence of a Neanderthal from the Altai Mountains. *Nature* **505,** 43–49 (2014).
3. Meyer, M. *et al.* A high-coverage genome sequence from an archaic Denisovan individual. *Science* **338,** 222–226 (2012).
4. Weiss, L. A. *et al.* Association between microdeletion and microduplication at 16p11.2 and autism. *N. Engl. J. Med.* **358,** 667–675 (2008).
5. Kumar, R. A. *et al.* Recurrent 16p11.2 microdeletions in autism. *Hum. Mol. Genet.* **17,** 628–638 (2008).
6. Huddleston, J. *et al.* Reconstructing complex regions of genomes using long-read sequencing technology. *Genome Res.* **24,** 688–696 (2014).
7. Johnson, M. E. *et al.* Positive selection of a gene family during the emergence of humans and African apes. *Nature* **413,** 514–519 (2001).
8. Zufferey, F. *et al.* A 600 kb deletion syndrome at 16p11.2 leads to energy imbalance and neuropsychiatric disorders. *J. Med. Genet.* **49,** 660–668 (2012).
9. Jacquemont, S. *et al.* Mirror extreme BMI phenotypes associated with gene dosage at the chromosome 16p11.2 locus. *Nature* **478,** 97–102 (2011).
10. Patterson, N., Richter, D. J., Gnerre, S., Lander, E. S. & Reich, D. Genetic evidence for complex speciation of humans and chimpanzees. *Nature* **441,** 1103–1108 (2006).
11. Auton, A. *et al.* A global reference for human genetic variation. *Nature* **526,** 68–74 (2015).
12. Sudmant, P. H. *et al.* Diversity of human copy number variation and multicopy genes. *Science* **330,** 641–646 (2010).
13. Lazaridis, I. *et al.* Ancient human genomes suggest three ancestral populations for present-day Europeans. *Nature* **513,** 409–413 (2014).
14. Fu, Q. *et al.* Genome sequence of a 45,000-year-old modern human from western Siberia. *Nature* **514,** 445–449 (2014).
15. Tishkoff, S. A. *et al.* The genetic structure and history of Africans and African Americans. *Science* **324,** 1035–1044 (2009).
16. Yang, M. A., Harris, K. & Slatkin, M. The projection of a test genome onto a reference population and applications to humans and archaic hominins. *Genetics* **198,** 1655–1670 (2014).
17. Hudson, R. R. Generating samples under a Wright-Fisher neutral model of genetic variation. *Bioinformatics* **18,** 337–338 (2002).
18. Ewing, G. & Hermisson, J. MSMS: a coalescent simulation program including recombination, demographic structure and selection at a single locus. *Bioinformatics* **26,** 2064–2065 (2010).
19. Vernot, B. *et al.* Excavating Neandertal and Denisovan DNA from the genomes of Melanesian individuals. *Science* **352,** 235–239 (2016).
20. Lappalainen, T. *et al.* Transcriptome and genome sequencing uncovers functional variation in humans. *Nature* **501,** 506–511 (2013).
21. Marchetto, M. C. *et al.* Differential L1 regulation in pluripotent stem cells of humans and apes. *Nature* **503,** 525–529 (2013).
22. Brawand, D. *et al.* The evolution of gene expression levels in mammalian organs. *Nature* **478,** 343–348 (2011).
23. Simons VIP Consortium. Simons Variation in Individuals Project (Simons VIP): a genetics-first approach to studying autism spectrum and related neurodevelopmental disorders. *Neuron* **73,** 1063–1067 (2012).
24. Nuttle, X. *et al.* Rapid and accurate large-scale genotyping of duplicated genes and discovery of interlocus gene conversions. *Nature Methods* **10,** 903–909 (2013).
25. Bersaglieri, T. *et al.* Genetic signatures of strong recent positive selection at the lactase gene. *Am. J. Hum. Genet.* **74,** 1111–1120 (2004).

26. Li, H., Mapolelo, D. T., Randeniya, S., Johnson, M. K. & Outten, C. E. Human glutaredoxin 3 forms [2Fe-2S]-bridged complexes with human BolA2. *Biochemistry* **51,** 1687–1696 (2012).
27. Li, H. & Outten, C. E. Monothiol CGFS glutaredoxins and BolA-like proteins: [2Fe-2S] binding partners in iron homeostasis. *Biochemistry* **51,** 4377–4389 (2012).
28. Kumánovics, A. *et al.* Identification of FRA1 and FRA2 as genes involved in regulating the yeast iron regulon in response to decreased mitochondrial iron-sulfur cluster synthesis. *J. Biol. Chem.* **283,** 10276–10286 (2008).
29. Haunhorst, P. *et al.* Crucial function of vertebrate glutaredoxin 3 (PICOT) in iron homeostasis and hemoglobin maturation. *Mol. Biol. Cell* **24,** 1895–1903 (2013).
30. Banci, L., Camponeschi, F., Ciofi-Baffoni, S. & Muzzioli, R. Elucidating the molecular function of human BOLA2 in GRX3-dependent anamorsin maturation pathway. *J. Am. Chem. Soc.* **137,** 16133–16143 (2015).

Supplementary Information is available in the online version of the paper.

Acknowledgements We thank families at the participating Simons Variation in Individuals Project (Simons VIP) and Simons Simplex Collection sites, as well as the Simons VIP Consortium. Approved researchers can obtain the Simons VIP data set, the Simons Simplex Collection data set and/or biospecimens by applying at https://base.sfari.org. We thank M. Chaisson for single-molecule, real-time WGS data, B. Vernot for archaic introgression data, B. J. Nelson and K. Munson for technical assistance, M. L. Gage for editorial comments and T. Brown for assistance with manuscript preparation. This work was supported by the Paul G. Allen Foundation (grant 11631 to E.E.E.), the Simons Foundation Autism Research Initiative (SFARI 303241 to E.E.E. and 274424 to A.R.), the US National Institutes of Health (NIH grant 2R01HG002385 to E.E.E.), the Swiss National Science Foundation (31003A_160203 and CRSII33-133044 to A.R.) and funds from NIH TR01 MH095741, the Helmsley Charitable Fund, the Mathers Foundation and the JPB Foundation (to F.H.G.). X.N. was supported by a US National Science Foundation Graduate Research Fellowship under grant DGE-1256082. G.G. was awarded a Pro-Women Scholarship from the Faculty of Biology and Medicine, University of Lausanne. M.H.D. is supported by US National Institute of Mental Health grant 1F30MH105055-01. O.P. is a recipient of a Human Frontier Science Program postdoctoral fellowship. L.B. is supported by EC grant N653706, project iNEXT. S.C.B. and F.C. were supported by an Ente Cassa di Risparmio grant (2013/7201). E.E.E. is an investigator of the Howard Hughes Medical Institute. The funders had no role in study design, data collection and analysis, decision to publish or preparation of the manuscript.

Author Contributions X.N., G.G., M.H.D., A.Re. and E.E.E. designed the study. X.N., G.G., M.H.D., M.M., J.H., L.D., L.H., C.Ba., A.Ra. and K.P. contributed to sequencing and assembly of haplotypes. X.N. developed the evolutionary model, with input from G.G. P.H.S. genotyped aggregate copy number from WGS data. X.N. and M.H.D. performed MIP experiments and analysed WGS data to genotype paralogue-specific copy number and refine rearrangement breakpoints. N.J. performed massively parallel sequencing. J.G.S., M.H.D. and X.N. performed population genetic simulations, with input from J.M.A. G.G. analysed RNA-seq data from LCLs, performed western blots and assessed the correlation of expression with copy number. I.N., C.Be. and M.C.N.M. performed and analysed RNA-seq experiments over *in vitro* differentiation of experimentally derived primate stem cells, with supervision from F.H.G. O.P., G.G. and X.N. analysed RNA-seq data from different human and nonhuman primate tissues. J.H. performed inversion density simulations using data provided by F.A. and M.V. G.C. and F.A. performed fluorescence *in situ* hybridization (FISH) experiments. F.C., S.C.B., H.A.F.S. and L.B. performed functional experiments and provided insights into potential effects of increased BOLA2 dosage. W.J.T. and C.T.A. constructed a bacterial artificial chromosome library. X.N. and E.E.E. wrote the paper, with input and approval from all co-authors.

Author Information Clone sequences, haplotype contig sequences and MIP data are available at the NCBI BioProject database under accession number PRJNA325679. RNA-seq data for neural progenitor cells and neurons are available at NCBI Gene Expression Omnibus under accession numbers GSE47626 and GSE83638. Patient WGS and MIP data are available at SFARI Base (https://sfari.org/resources/sfari-base) under accession numbers SFARI_SVIP_WGS_1 and SFARI_SVIP_MIPS_1. Reprints and permissions information is available at www.nature.com/reprints. The authors declare competing financial interests: details are available in the online version of the paper. Readers are welcome to comment on the online version of the paper. Correspondence and requests for materials should be addressed to E.E.E. (eee@gs.washington.edu) or A.R. (alexandre.reymond@unil.ch).

Reviewer Information *Nature* thanks D. Conrad, D. Haussler, C. Tyler-Smith and the other anonymous reviewer(s) for their contribution to the peer review of this work.

METHODS

No statistical methods were used to predetermine sample size. The experiments were not randomized. The investigators were not blinded to allocation during experiments and outcome assessment.

Single-molecule, real-time sequencing was used to generate high-quality sequence[6] from bacterial artificial chromosome clones obtained from genomic libraries. Clone sequences were assembled using HGAP and error-corrected using Quiver[31]. Contig assembly was performed using Sequencher (Gene Codes Corporation, Ann Arbor, Michigan) and validated by FISH. Copy number genotyping of genes and segmental duplications was performed using a read-depth method[12] and WGS data from humans[32,33], nonhuman primates[34] and archaic genomes[2,3,13,14], as well as single-molecule MIPs[35] targeted to paralogous sequence variants[24]. We estimated evolutionary timing of segmental duplication events on the basis of comparative sequencing and phylogenetic analyses (neighbour-joining method), adjusting branch lengths for trees that failed the Tajima's relative rate test and assuming divergence times of 6 Ma (human–chimpanzee)[10] and 15 Ma (human–orangutan). Evolutionary conservation analysis of *BOLA2* was performed by maximum likelihood (PAML). Likelihoods of *BOLA2B* fixation under different scenarios were assessed using the coalescent simulators *ms*[17] and *msms*[18], adapting a previously published demographic model[16]. *BOLA2* copy number estimates were correlated (Pearson's *r*) using RNA-seq quantifications[20] (PEER-normalized RPKM) and western blot BOLA2 densities in human LCLs grown in complete RPMI medium and lysed in RIPA buffer. After SDS–PAGE and transfer to PVDF membrane, blots were incubated with an anti-BOLA2 antibody (Santa Cruz Biotechnology, Dallas, Texas) and an anti-actin antibody (Sigma) for normalization purposes. Band densities were quantified using the Bio1D software. *BOLA2* coding DNA sequence (CDS) was cloned using the Gateway system (Invitrogen, Carlsbad, California). HeLa cells were transfected with cytomegalovirus-*BOLA2* CDS (both 10 and 17 kDa forms) and analysed by western blotting. *BOLA2* gene models were established via RT–PCR, cloning and capillary sequencing. RNA-seq data were generated from previously described embryonic stem cell and iPSC lines[21], as well as iPSC lines differentiated into neural progenitor cells and neurons. *BOLA2* mRNA expression was quantified in transcripts per million with Kallisto[36] (version 0.42.1) using a custom catalogue of transcripts including all human RefSeq transcripts with the three *BOLA2* isoforms. Breakpoints of chromosome 16p11.2 rearrangements were refined using Illumina whole-genome shotgun sequencing[37,38] and single-molecule MIP analysis[24,35,37] of patient DNA obtained from the Simons VIP[23] and Simons Simplex Collection[39]. All procedures for clinical assessment and blood extraction were approved by the institutional review boards of participating institutions, and informed consent was obtained for participation in this research.

31. Chin, C. S. *et al.* Nonhybrid, finished microbial genome assemblies from long-read SMRT sequencing data. *Nature Methods* **10,** 563–569 (2013).
32. The 1000 Genomes Project Consortium. An integrated map of genetic variation from 1,092 human genomes. *Nature* **491,** 56–65 (2012).
33. Sudmant, P. H. *et al.* Global diversity, population stratification, and selection of human copy-number variation. *Science* **349,** aab3761 (2015).
34. Prado-Martinez, J. *et al.* Great ape genetic diversity and population history. *Nature* **499,** 471–475 (2013).
35. Hiatt, J. B., Pritchard, C. C., Salipante, S. J., O'Roak, B. J. & Shendure, J. Single molecule molecular inversion probes for targeted, high-accuracy detection of low-frequency variation. *Genome Res.* **23,** 843–854 (2013).
36. Bray, N., Pimentel, H., Melsted, P. & Pachter, L. Near-optimal RNA-seq quantification. Preprint at http://arxiv.org/abs/1505.02710 (2015).
37. Nuttle, X., Itsara, A., Shendure, J. & Eichler, E. E. Resolving genomic disorder-associated breakpoints within segmental DNA duplications using massively parallel sequencing. *Nature Protocols* **9,** 1496–1513 (2014).
38. Antonacci, F. *et al.* Palindromic *GOLGA8* core duplicons promote chromosome 15q13.3 microdeletion and evolutionary instability. *Nature Genet.* **46,** 1293–1302 (2014).
39. Fischbach, G. D. & Lord, C. The Simons Simplex Collection: a resource for identification of autism genetic risk factors. *Neuron* **68,** 192–195 (2010).

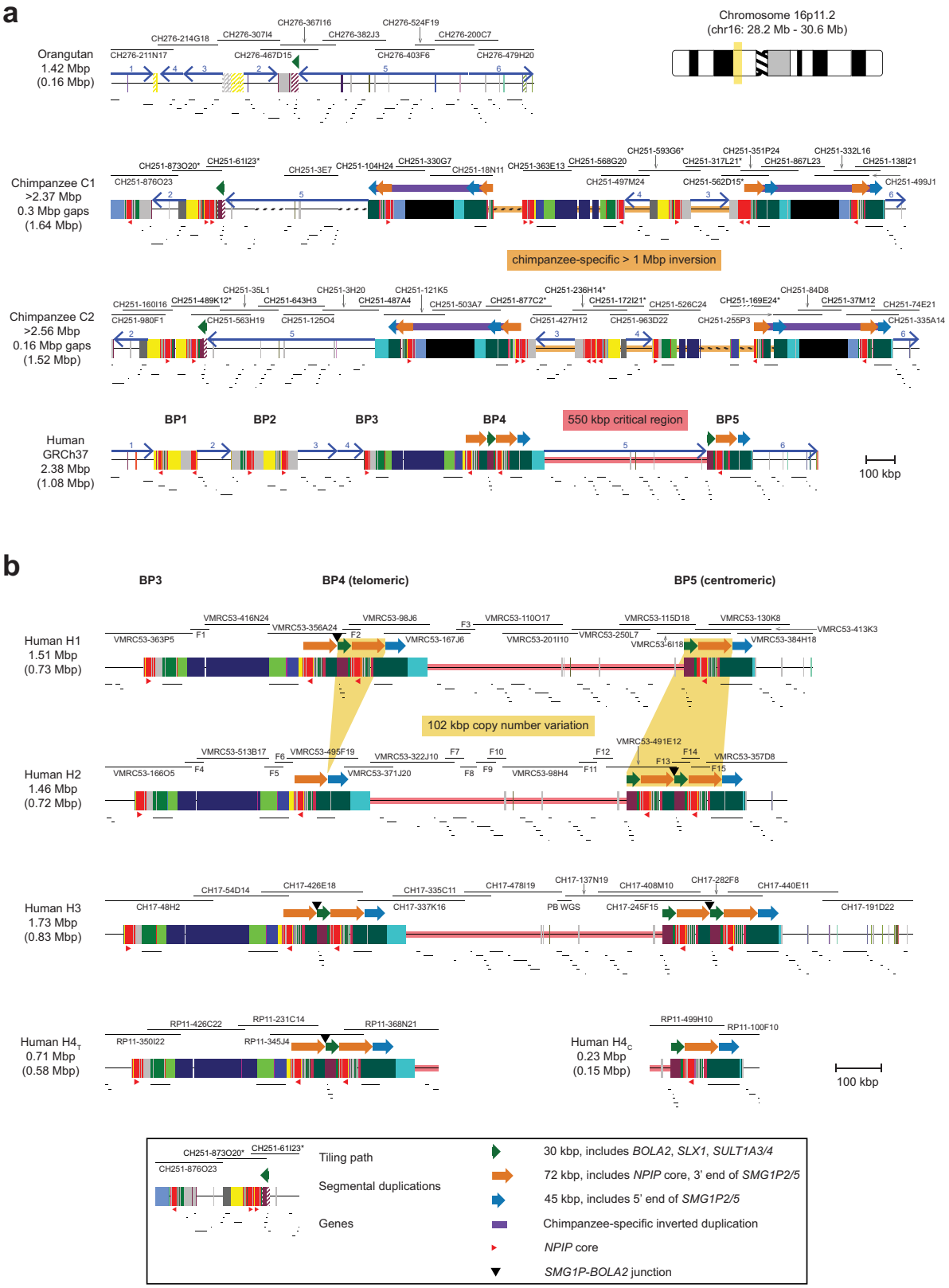

Extended Data Figure 1 | See next page for caption.

Extended Data Figure 1 | Comparative sequence analysis of chromosome 16p11.2 among apes. a, Genomic organization of chromosome 16p11.2 for one orangutan and two chimpanzee haplotypes and the human reference haplotype (GRCh37 chr16:28195661–30573128; see ideogram for approximate chromosomal location). Blocks of segmental duplications within this locus mediate recurrent rearrangements in humans; thus, these blocks have been defined as breakpoint regions BP1–BP5 (ref. 8). The ~550-kbp critical region (pink) and a >1-Mbp chimpanzee-specific inversion polymorphism (orange) are highlighted. Tiling paths of sequenced clones are indicated above each haplotype, with chimpanzee clones that could not be fully resolved marked with asterisks. Coloured boxes and thick arrows indicate the extent and orientation of segmental duplications (with different colours denoting duplicons from different ancestral genomic loci and hashed boxes indicating sequence duplicated in humans but not in the species represented). Thin numbered arrows show orientations of gene-rich regions of unique sequence. Numbers (left) indicate the size of each orthologous haplotype, with the number of segmentally duplicated base pairs shown in parentheses. Note that, for chimpanzee, these sizes are lower bounds owing to gaps in the contigs (dotted line sections) and the contigs not reaching unique sequence beyond BP1 (that is, unique region 1). **b**, Distinct human structural haplotypes over the chromosome 16p11.2 critical region and flanking sequences (three complete haplotypes extending from unique sequence distal to BP3 to unique sequence proximal to BP5 and one partial haplotype including BP3–BP4 and BP5 sequence contigs). High-quality sequence for each haplotype was generated by sequencing a total of 40 bacterial artificial chromosomes and 15 fosmids from three different human genomic libraries. Regions of CNV (highlighted in yellow along the first two haplotypes) occur on both sides of the critical region and involve the same 102-kbp unit in direct orientation, including a 30-kbp block containing *BOLA2* and two other genes and a 72-kbp block harbouring a partial segmental duplication of *SMG1* (*SMG1P*). Expansion and contraction of this cassette underlie hundreds of kilobase pairs of structural diversity between human haplotypes. *BOLA2* paralogue-specific copy number genotype data suggest that H1 and H3 probably represent the most common haplotype structures in humans.

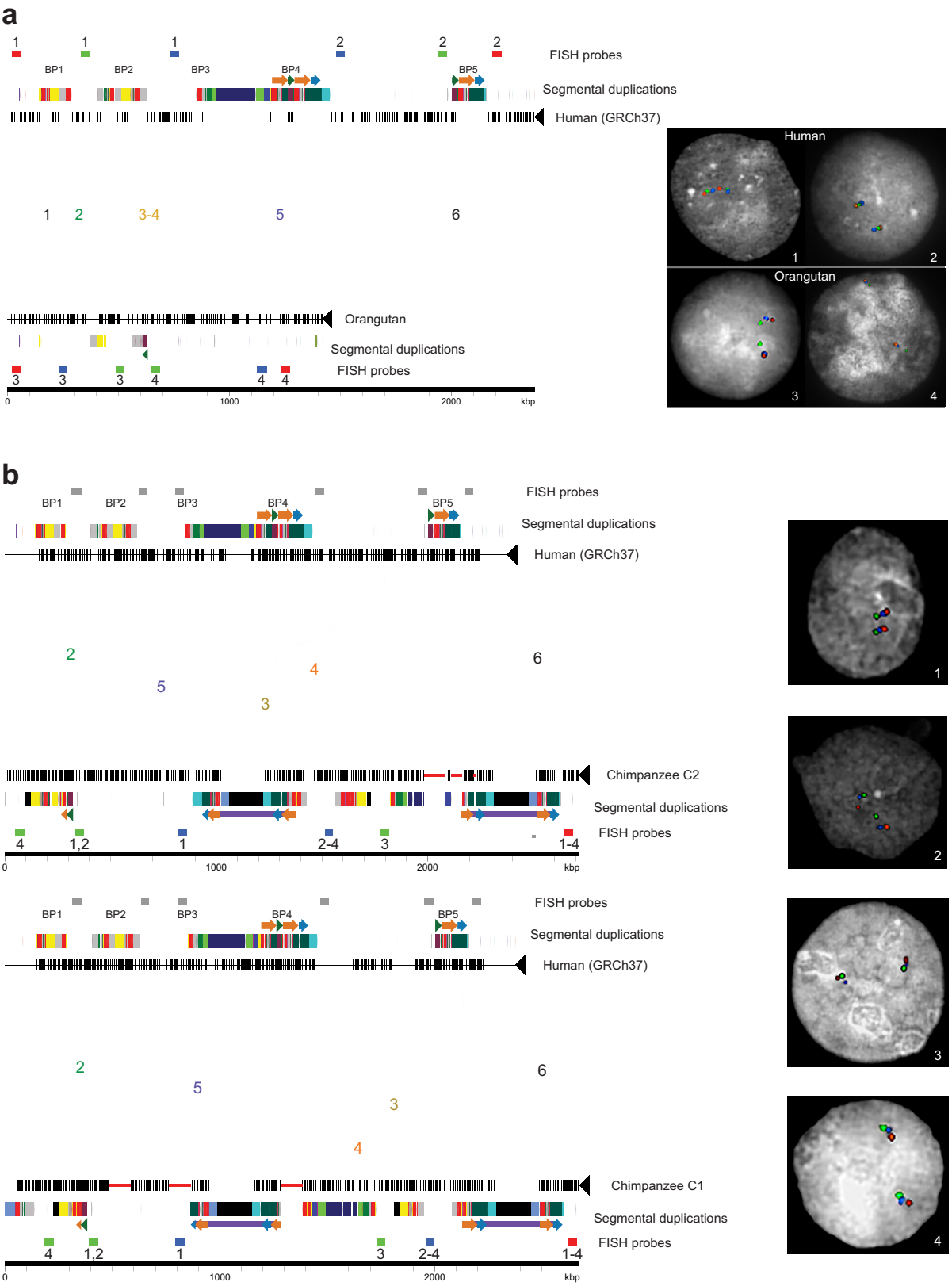

Extended Data Figure 2 | See next page for caption.

Extended Data Figure 2 | Comparison of chromosome 16p11.2 structure between apes. a, Sequences (thin horizontal lines) from human (GRCh37 chr16:28195661–30573128) and orangutan (contig sequence) at chromosome 16p11.2 are compared using Miropeats ($s = 1{,}000$) and annotated with locations of human segmental duplications and FISH probes used to validate the organization of the region. Lines connecting the sequences show regions of homology, and line colours highlight differences in the order and orientation of distinct gene-rich regions of unique sequence across the locus (numbered 1–6). Numbers below FISH probes correspond to numbers within the images on the right, specifying which probes were used in each experiment. Experiment 1 used the same probes as experiment 3, and experiment 2 used the same probes as experiment 4. Three-colour interphase FISH on human and orangutan chromosomes confirms the accuracy of our assembled orangutan contig. **b**, Sequences (thin horizontal lines) from human (GRCh37 chr16:28195661–30573128) and two chimpanzee structural haplotypes at chromosome 16p11.2 are compared using Miropeats ($s = 1{,}500$) and annotated with locations of human segmental duplications and FISH probes used to validate the organization of the region. Thick red horizontal lines indicate gaps in the chimpanzee contigs, and black boxes correspond to chimpanzee-specific segmental duplications (that is, sequences not duplicated in humans). Lines connecting the sequences show regions of homology, and line colours highlight differences in the order and orientation of distinct gene-rich regions of unique sequence across the locus (numbered 2–6). Numbers below FISH probes correspond to numbers within the images on the right, specifying which probes were used in each experiment. Grey rectangles show mapping locations of FISH probes in human. Three-colour interphase FISH on chimpanzee chromosomes confirms the accuracy of our assembled contigs.

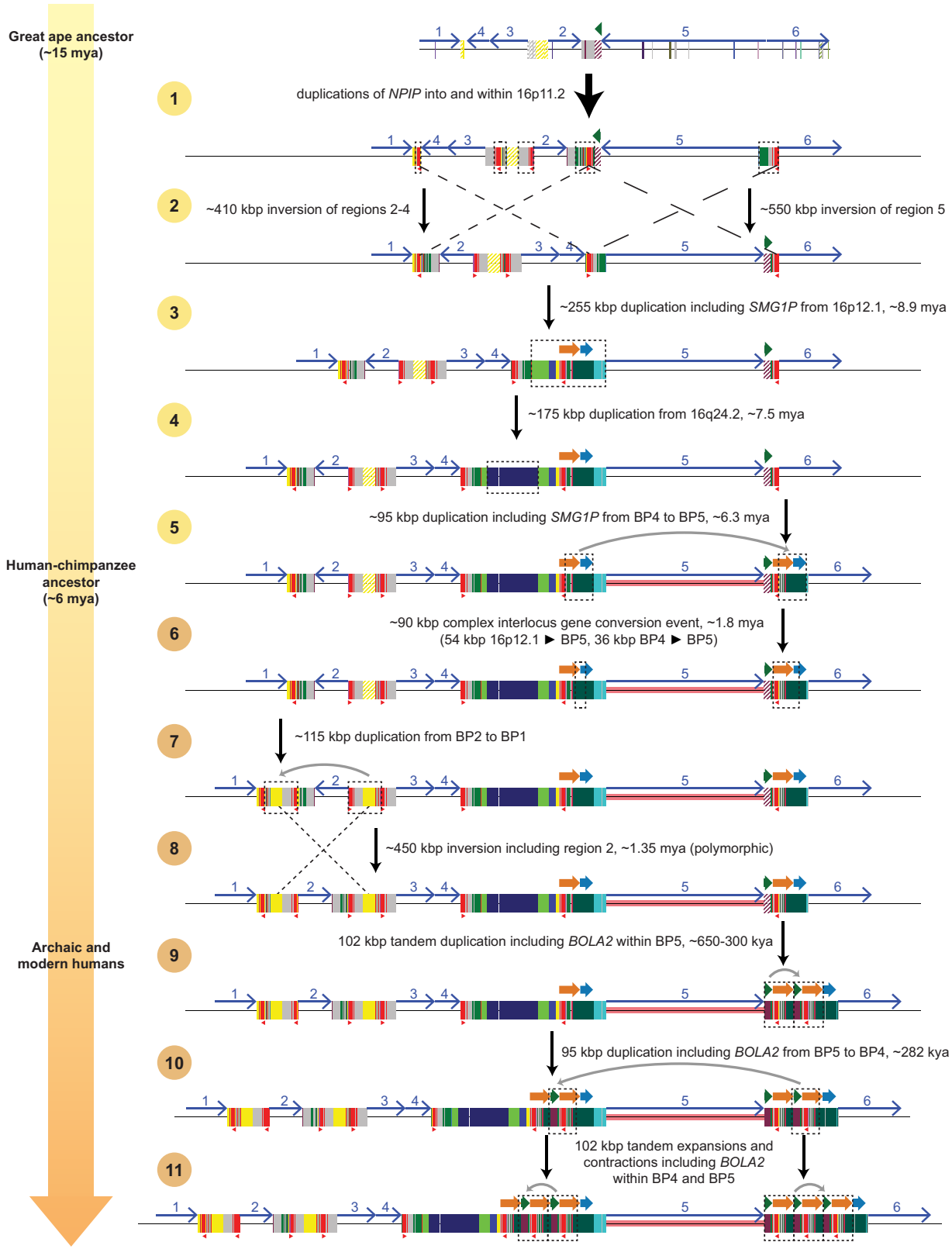

Extended Data Figure 3 | Dynamic evolution of human chromosome 16p11.2. a, A model for the evolution of the chromosome 16p11.2 BP1–BP5 region[8] during great ape evolution. The schematic depicts structural changes over time leading to the present-day human architecture (see Supplementary Information for details). The orangutan structure (top) is largely devoid of segmental duplications and deemed to represent the ape ancestral organization because it is conserved with mouse. Subsequent steps were inferred on the basis of phylogenetic reconstruction, origins of the duplicated sequences and the most parsimonious path with respect to changes in gene order (inversions). (See Supplementary Information for a detailed discussion of all supporting evidence and confidence levels for each step.) Note that, without access to genomes containing intermediate chromosome 16p11.2 structures, it is impossible to know with certainty the entire step-by-step evolutionary history. Some details presented here may not be accurate. mya, million years ago; kya, thousand years ago.

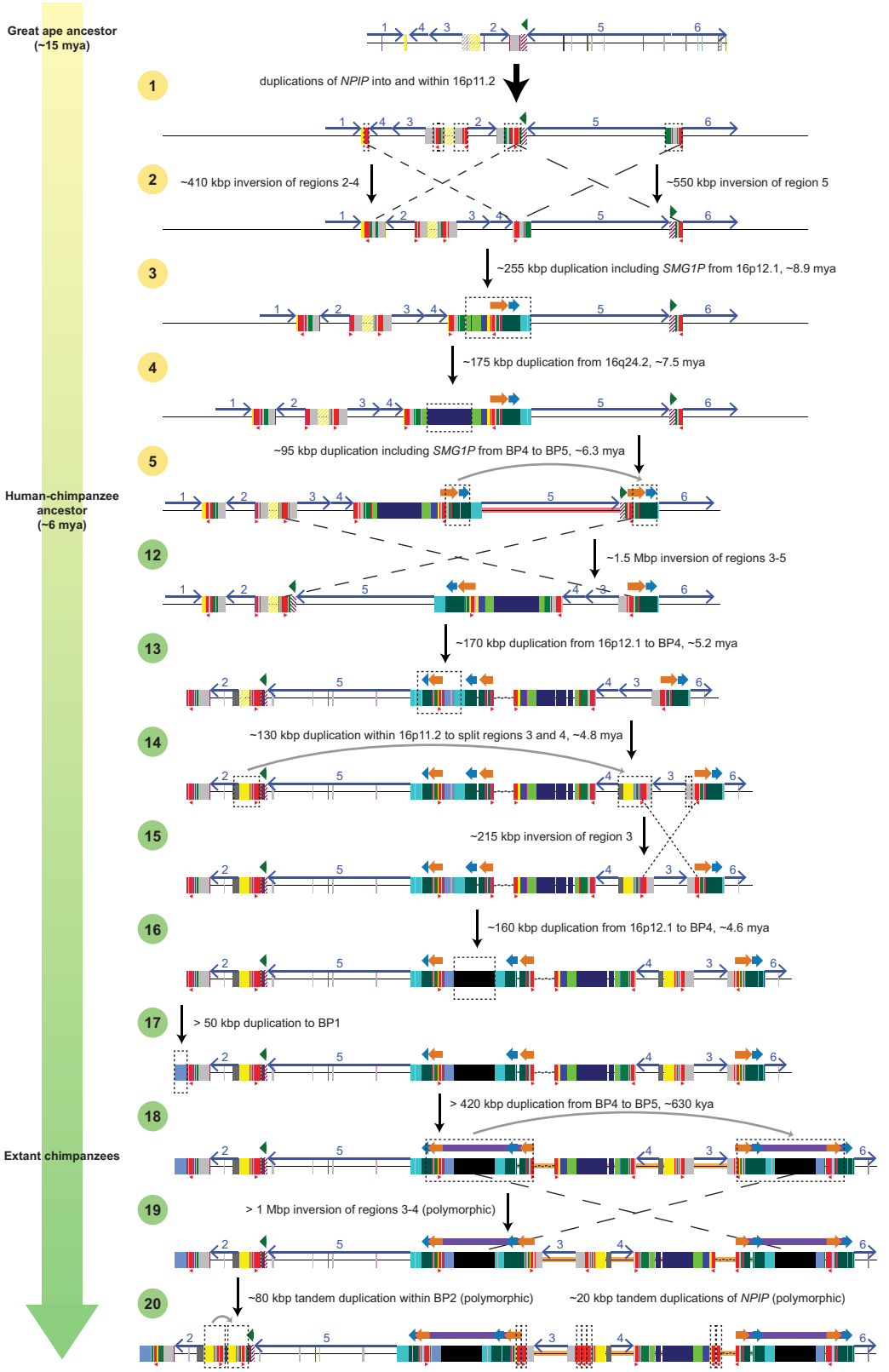

Extended Data Figure 4 | Dynamic evolution of chimpanzee chromosome 16p11.2. A model for the evolution of the chromosome 16p11.2 BP1–BP5 region[8] during great ape evolution. The schematic depicts structural changes over time leading to the present-day chimpanzee architecture (see Supplementary Information for details and discussion of all supporting evidence and confidence levels for each step).

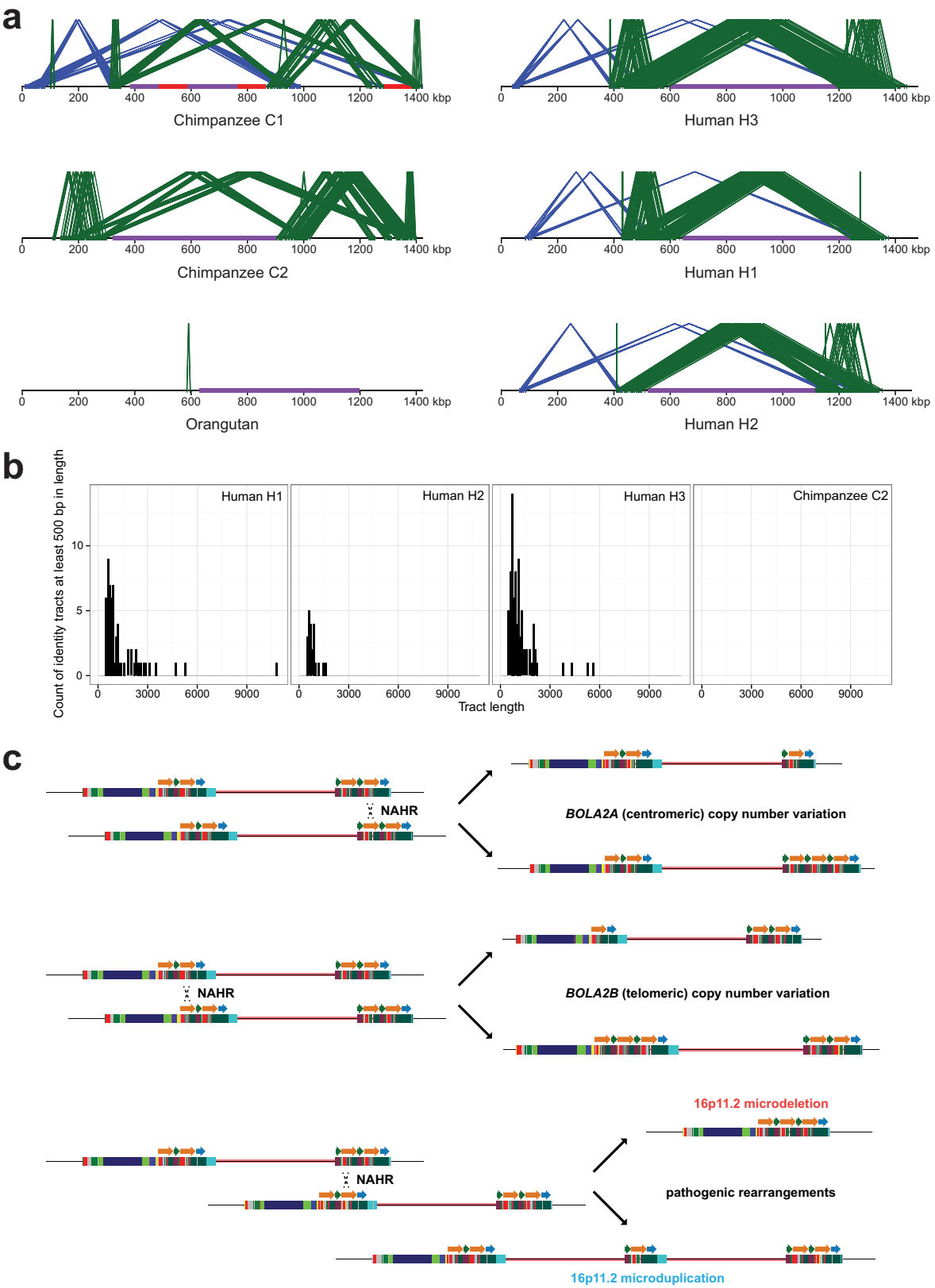

Extended Data Figure 5 | See next page for caption.

Extended Data Figure 5 | Comparison of duplications around the chromosome 16p11.2 autism critical region among apes and nonallelic homologous recombination (NAHR) model underlying CNV at human chromosome 16p11.2. a, Local directly oriented (green) and inversely oriented (blue) intrachromosomal segmental duplications flanking the chromosome 16p11.2 autism critical region (purple) are visualized using Miropeats (s = 1,000). Gaps in the chimpanzee C1 contig are shown in red. The smaller size (<50 kbp) and lower average sequence identity (at most 98.6%) of directly oriented duplications flanking the critical region in chimpanzee compared with human haplotypes including *BOLA2* on both sides of the critical region (at least 147 kbp of directly oriented duplications having at least 99.3% average sequence identity) suggest that susceptibility to NAHR resulting in microdeletions and microduplications at this locus evolved specifically in humans. **b**, Perfect sequence identity tract lengths (>500 bp) within directly oriented duplications flanking the critical region for human versus chimpanzee. Histograms show counts of tracts of perfect sequence identity (lacking single-nucleotide variants and indels) between directly oriented segmental duplications of interest within each indicated haplotype and the distribution of these tracts over different size ranges. Human haplotypes having *BOLA2* on both sides of the critical region (H1 and H3) contain the highest number of such tracts and the longest such tracts, including one tract spanning 10,774 bp. In contrast, the longest tract of perfect sequence identity between duplications of interest in chimpanzee (considering both the C1 and C2 haplotypes) spans 450 bp. **c**, NAHR model underlying normal and disease-associated CNV at human chromosome 16p11.2.

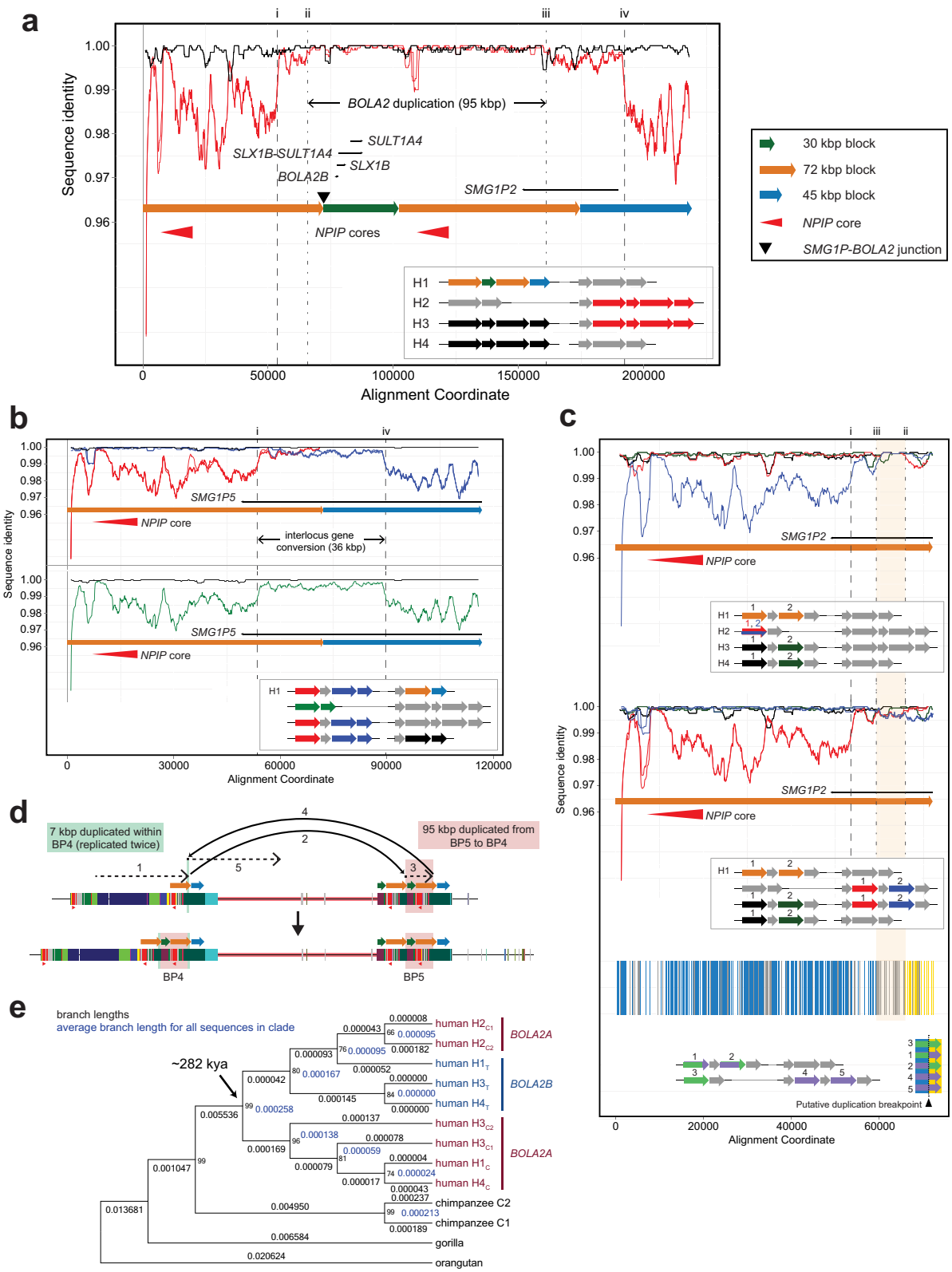

Extended Data Figure 6 | See next page for caption.

Extended Data Figure 6 | Sequence refinement of interspersed *BOLA2* duplication breakpoints, inference of *BOLA2* duplication mechanism and phylogenetic *BOLA2* duplication timing. a, H1 human BP4 sequence (orange, green, orange and blue arrows in inset) was aligned to its allelic (black arrows in inset) and paralogous (red arrows in inset) counterparts. The sequence identity for each alignment was computed and plotted over 2-kbp windows, sliding by 100 bp. Black lines indicate sequence identity for allelic comparisons, whereas red lines correspond to paralogous comparisons. While the allelic comparisons exhibit uniform, near-perfect sequence identity across the entirety of the alignment, paralogous comparisons reveal three distinct levels of sequence identity, with the highest level in the middle. This pattern suggests that the *BOLA2* duplication (highest-identity region, 95 kbp) landed within an evolutionarily older segmental duplication having paralogues at BP4 and BP5. Dashed vertical lines (numbered i–iv) indicate putative breakpoints for events that occurred after this older segmental duplication. Junction sequence from the BP5 102-kbp tandem duplication (that is, the *SMG1P*–*BOLA2* junction) was clearly included in the 95-kbp duplication from BP5 to BP4. **b**, Alignment of BP4 sequences containing the putative left (red arrows in inset) and right (dark blue arrows in inset) *BOLA2* duplication breakpoints to the BP5 paralogue associated with the evolutionarily older segmental duplication (orange and light blue arrows in inset) and sliding window sequence identity analysis supports the hypothesis outlined above. Sequence identity lines for comparisons involving left and right BP4 sequences intersect in the vicinity of the hypothesized *BOLA2* duplication breakpoints. Comparing this result with the same analysis of the human H2 BP4 sequence lacking *BOLA2* (green arrows in inset and green identity line) suggests this BP4 sequence represents the ancestral state of BP4 before the *BOLA2* duplication arrived. Thus, two levels of sequence identity existed between BP4 and BP5 before the *BOLA2* duplication, consistent with an interlocus gene conversion event. **c**, Alignment of BP4 sequences (orange arrows in insets) containing the putative *BOLA2* duplication breakpoints to their ancestral BP4 (top plot) and their ancestral BP5 (middle plot) counterparts and sliding window sequence identity analysis reveals an ~7-kbp window (highlighted in orange) defining the *BOLA2* duplication breakpoints. Analysis of the underlying multiple sequence alignment (Supplementary Table 5) identified positions with signatures informative for breakpoint localization (blue vertical lines, left BP4 72-kbp block outside the *BOLA2* duplication and right BP4 72-kbp block within the *BOLA2* duplication; yellow vertical lines, left BP4 72-kbp block within the *BOLA2* duplication and right BP4 72-kbp block outside the *BOLA2* duplication). Grey vertical lines indicate positions showing signatures of interlocus gene conversion. As both left and right 72-kbp block BP4 sequences within the ~7-kbp window are more highly identical to ancestral BP4 sequence (20/24 informative positions match the ancestral BP4 sequence) than to ancestral BP5 sequence, it is likely that this interval was involved in the *BOLA2* duplication but duplicated only within BP4. Its boundaries define the most likely *BOLA2* duplication breakpoints, and this pattern of sequence identity suggests a template-switching replicative mechanism as most probably underlying the *BOLA2* duplication event. **d**, Template-switching model for the formation of *BOLA2B*. This mechanism was inferred from the sequence identity analyses in **a**–**c** and from analysis of a multiple sequence alignment (Supplementary Table 5). **e**, Phylogenetic characterization of the 95-kbp duplication containing *BOLA2* from BP5 to BP4. Cladogram representation of an unrooted neighbour-joining phylogenetic tree based on a 21,102-bp multiple sequence alignment spanning *BOLA2* and most of the 30-kbp block including human sequences from BP4 and BP5 and single-copy orthologous sequences from chimpanzee, gorilla and orangutan. Branch lengths (substitutions per site) are shown on each branch (black decimal numbers), and bootstrap support is indicated (black integers at nodes). Blue numbers correspond to nodes and indicate average branch lengths for all sequences in corresponding clades. Branch lengths were used to estimate the time corresponding to the 95-kbp duplication containing *BOLA2* from BP5 to BP4 as shown.

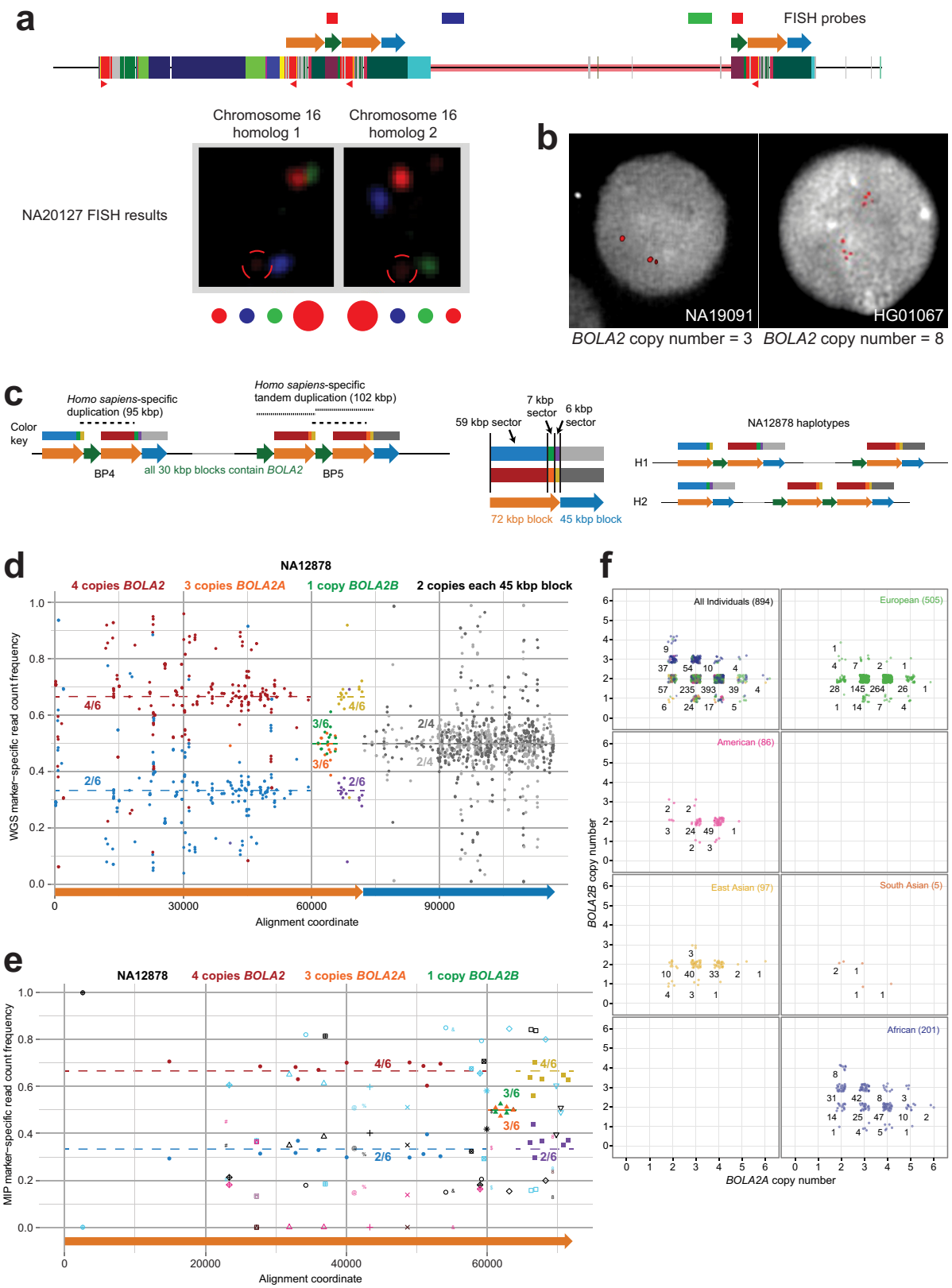

Extended Data Figure 7 | See next page for caption.

Extended Data Figure 7 | Analyses of *BOLA2* aggregate and paralogue-specific CNV in humans. a, Interphase FISH confirms both *BOLA2A* and *BOLA2B* show CNV. Previous interphase FISH analysis (data not shown) suggests the individual NA20127 has six total copies of *BOLA2*. Diagram outlines a three-colour FISH assay including two probes (blue, green) targeting sequences within the autism critical region and one probe (red) targeting ~18-kbp of sequence (including *BOLA2*) over the 30-kbp duplication block. Signals from the red probe are detected on the telomeric (BP4) and centromeric (BP5) sides of the critical region (adjacent to the blue and green probes, respectively) on both chromosome 16 homologues. However, the red probe signal intensity is strongest adjacent to the green probe for one homologue but, in contrast, is strongest adjacent to the blue probe for the other chromosome 16 homologue, consistent with higher *BOLA2A* copy number in the first case and higher *BOLA2B* copy number in the second case. These data indicate that individual NA20127 has three copies each of *BOLA2A* and *BOLA2B*. This differential signal intensity pattern does not result from an inversion of the chromosome 16p11.2 critical region in this individual, as data from another FISH experiment (data not shown) refute this possibility. Information on probes used in these FISH experiments is provided in Supplementary Table 2. **b**, Interphase FISH experiments using a probe targeting *BOLA2* and surrounding sequence for individuals having the lowest (three) and highest (eight) confirmed aggregate *BOLA2* copy numbers. **c**, Left and middle schematics detail three distinct sectors of the 72-kbp blocks (orange arrows). Each block has paralogous sequence variants that are informative for particular region(s) compared with others in chromosome 16p11.2. These markers are colour-coded into three sectors within the 72-kbp block of paralogy (a 59-kbp sector, blue and red boxes; a 7-kbp sector, green and orange boxes; and a 6-kbp sector, purple and yellow boxes), indicating which particular regions they distinguish. Right schematic shows known haplotype structures for individual NA12878. **d**, Analysing WGS data from NA12878 yields copy number estimates for *BOLA2A* and *BOLA2B* that match the known *BOLA2* paralogue-specific copy number (PSCN) for this individual. Each point shows a relative marker-specific read count frequency (*y* axis) and its position within the duplication blocks (*x* axis). Point colours correspond to different marker sets for each sector, as diagrammed in **c**. Fractions indicate the relative copy number of each marker set. Estimates of 4/6 (red marker set) versus 2/6 (blue marker set) for the 59-kbp sector confirms the sequenced architecture (**c**) with an aggregate of four *BOLA2* copies, and the estimate of 3/6 (orange marker set) confirms three copies of *BOLA2A*. WGS analysis also yields accurate PSCN estimates for the 45-kbp block. **e**, Using MIPs, we employed the same relative read-depth strategy. Genotyping results for the same sample as in **d** are shown, with additional markers (points not colour-coded as in **c** and **d**) added on the basis of polymorphic variants (symbols indicate different patterns of presence/absence among 72-kbp blocks, considering all such blocks from our four contiguous human haplotypes). MIP genotypes confirm WGS estimates (in **d**). **f**, *BOLA2* PSCN genotypes (points, jittered around their integer values for clarity) were inferred from MIP sequence data for 894 humans. Numbers indicate total counts of individuals in each population having a particular *BOLA2* PSCN genotype. Low-confidence estimates were excluded.

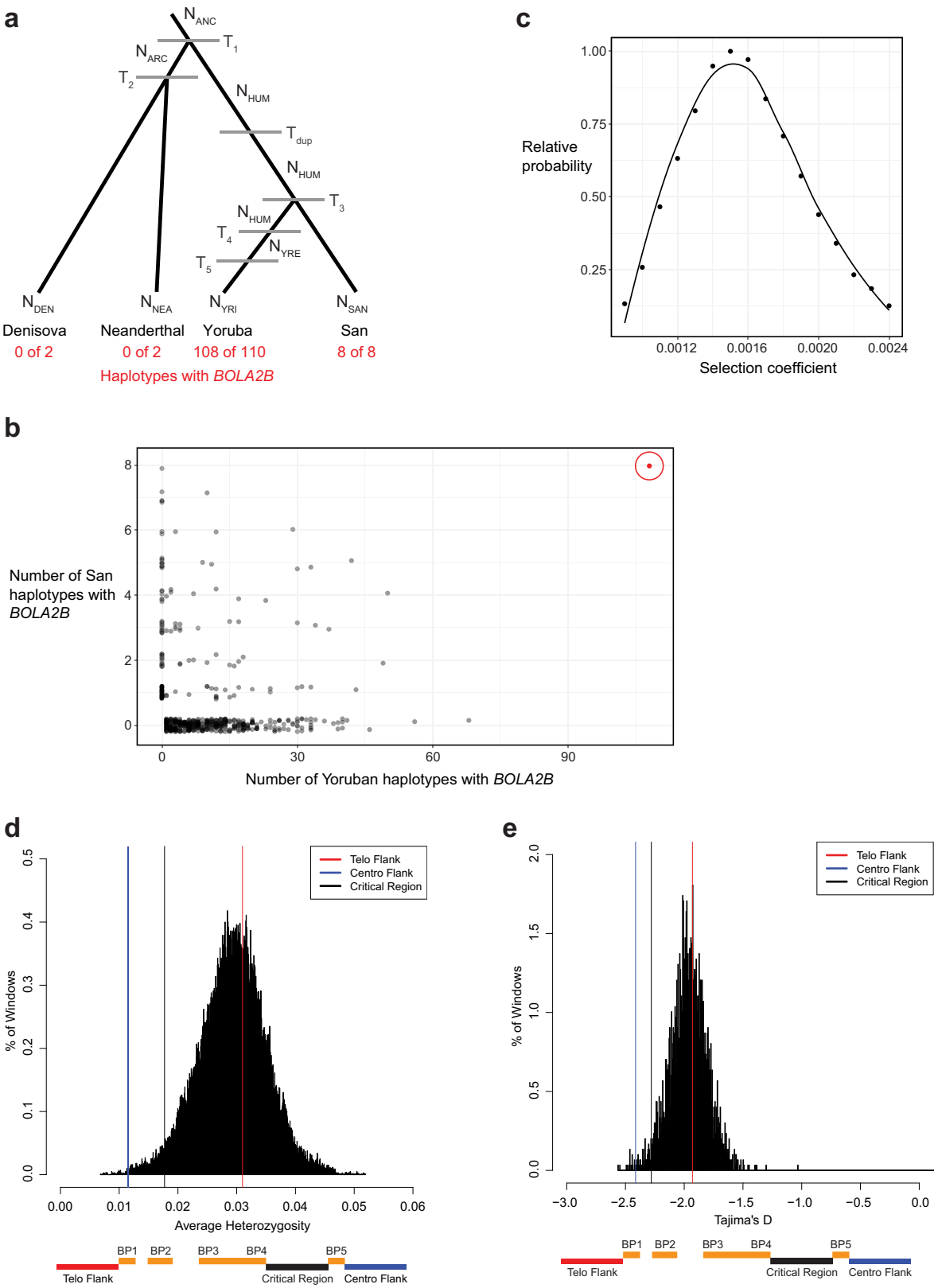

Extended Data Figure 8 | See next page for caption.

Extended Data Figure 8 | Population genetic modelling of the *BOLA2B* duplication and critical region analyses. a, Demographic model (adapted from ref. 16) used to simulate *BOLA2B* evolution under different scenarios. N_{ANC}, effective population size of *Homo* ancestor, 21,600. N_{ARC}, effective population size of Neanderthal-Denisova ancestor, 500. N_{HUM}, effective population size of human ancestor, 24,000. N_{YRE}, effective size of Yoruban population after expansion, 45,000. N_{DEN}, effective population size of Denisova, 500. N_{NEA}, effective population size of Neanderthal, 500. N_{YRI}, effective size of extant Yoruban population, 10,000. N_{SAN}, effective size of extant San population, 10,000. T_1, time of archaic hominin divergence from modern humans, 650,000 years. T_2, time of Neanderthal–Denisova divergence, 525,000 years. T_{dup}, time of formation of *BOLA2B*, 282,000 years. T_3, time of Yoruban-San divergence, 200,000 years. T_4, time of Yoruban population expansion, 157,500 years. T_5, time of Yoruban population decline, 37,500 years. **b**, Simulation results ($n = 1{,}000{,}000$) assuming that the duplication that formed *BOLA2B* occurred once, 282 ka, along the modern human ancestral lineage and evolved under neutrality compared with the observed genotype frequencies of *BOLA2B* in 8 San and 110 Yoruban haplotypes. Nearly all (999,531) simulations resulted in *BOLA2B* being lost from both populations; results from the remaining 469 simulations (black) are shown alongside the observed data (red, circled). Under this simple neutral model incorporating *BOLA2B* age, the observed *BOLA2B* frequency is never approached. **c**, Simulation was repeated exploring a range of selection coefficients from 0.0009 to 0.0024 (increments of 0.0001), and the relative probability of the observed data under each scenario was calculated as the proportion of simulations yielding the observed *BOLA2B* genotypes among simulations where *BOLA2B* was not lost relative to the maximum such proportion for any single selection coefficient considered. The maximum likelihood estimate for the selection coefficient was $s = 0.0015$. Smoothed line is the LOESS regression curve. **d**, Low average heterozygosity of the chromosome 16p11.2 BP4–BP5 critical region. Distribution of average heterozygosity values for 100,000 ~550-kbp regions of unique sequence randomly sampled with replacement from the autosomal genome compared with average heterozygosity values for the critical region (black line) and flanking unique sequences (coloured lines). The critical region lies in the bottom 2.6% of the distribution, showing low diversity consistent with potential positive selection. Bottom schematic indicates locations of the critical region and flanking unique regions in relation to segmental duplications across the locus—note that *BOLA2A* is located at BP5 and *BOLA2B* at BP4. Telo, telomeric; Centro, centromeric. **e**, Low Tajima's *D* score for the chromosome 16p11.2 BP4–BP5 critical region. Distribution of Tajima's *D* scores for 2,987 non-overlapping ~550-kbp regions across the genome compared with Tajima's *D* scores for the critical region (black line) and flanking unique sequences (coloured lines). The critical region lies in the bottom 2.7% of the distribution, consistent with possible positive selection. The distribution is centred near −2 rather than 0 because most single-nucleotide variants in the 1000 Genomes Project data set are rare variants having arisen during the large expansions of human populations over the past 100,000 years. Bottom schematic indicates locations of the critical region and flanking unique regions in relation to segmental duplications across the locus.

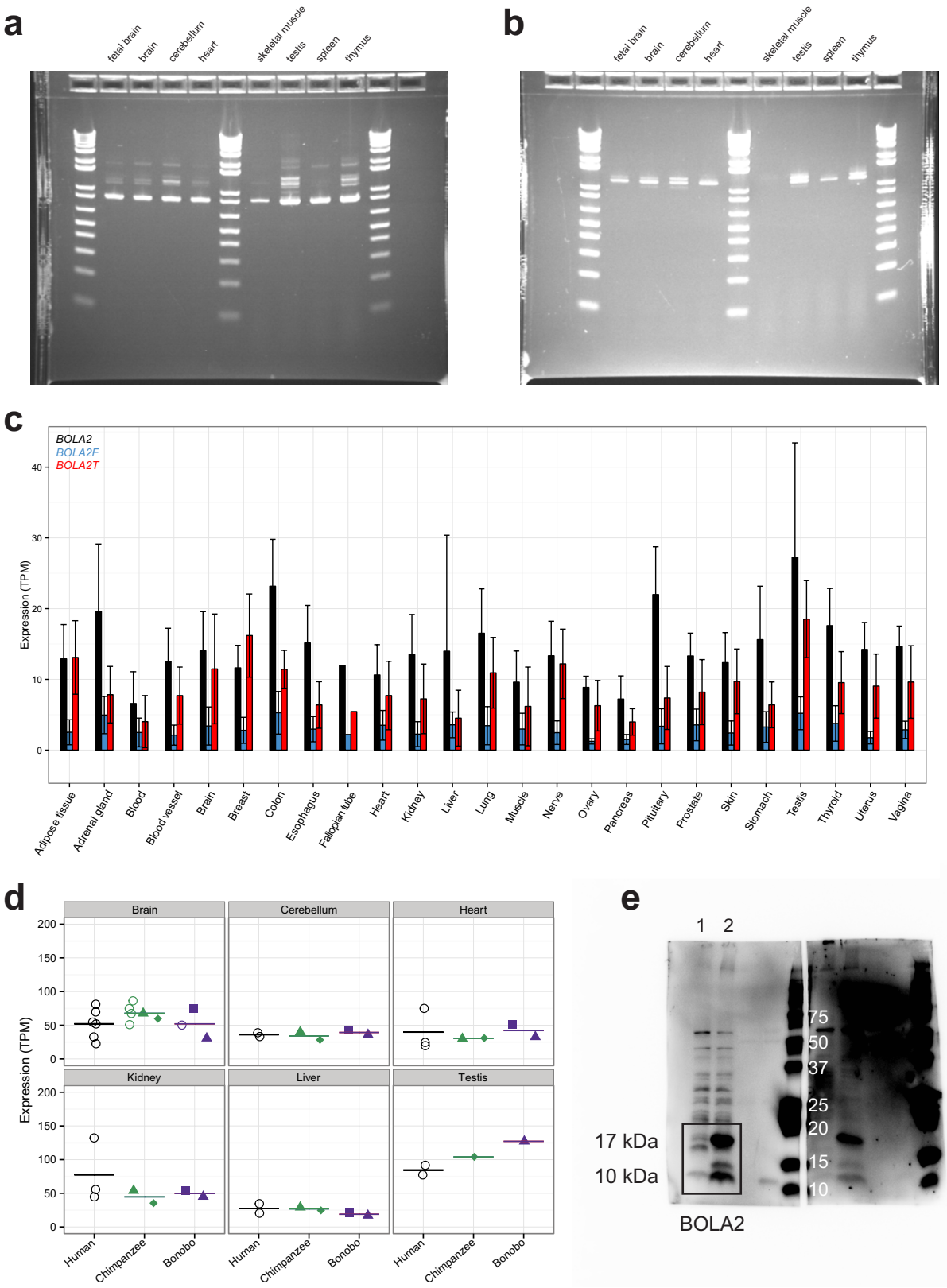

Extended Data Figure 9 | See next page for caption.

Extended Data Figure 9 | *BOLA2* expression and antibody validation. **a**, RT–PCR expression profile for canonical *BOLA2*. The expected product size for canonical *BOLA2* (838 bp) was observed in all eight human tissues; 1 kb + DNA ladder (Thermo Fisher). **b**, RT–PCR expression profile for *BOLA2-SMG1* fusion product. The expected product size for the *BOLA2* fusion transcript (1,239 bp) was observed as a doublet in all tissues except skeletal muscle. Intensity of upper band differs between tissues; 1 kb + DNA ladder (Thermo Fisher). **c**, *BOLA2* RNA-seq expression analysis. Canonical (*BOLA2*) and fusion transcripts (*BOLA2F*, *BOLA2T*) were assessed across 25 humans from GTEx RNA-seq data. Bar heights indicate mean expression levels for each tissue in transcripts per million with standard errors shown (error bars). Colours correspond to different *BOLA2* isoforms as indicated. **d**, *BOLA2* expression among primates in six adult tissues. Each point indicates a *BOLA2* expression estimate from a single tissue sample, with samples obtained from a total of 18 humans, 6 chimpanzees and 3 bonobos. Open circles correspond to individuals analysed in a single experiment, while closed shapes denote data from multiple experiments involving the same individual, with each distinct colour plus shape pattern showing all experiments for a particular individual. Horizontal lines show mean expression values for each species and tissue. Combined with our expression analyses of iPSCs, these data show *BOLA2* expression differs substantially between human, chimpanzee and bonobo only in stem cells. **e**, Western blotting of HeLa cells transfected with the human *BOLA2* annotated CDS and probed with an anti-BOLA2 antibody (Sc-163747). Whole-cell lysates of HeLa cells non-transfected with the overexpression construct (lane 1) and transfected with the human *BOLA2* annotated CDS (lane 2) were probed with anti-BOLA2 antibody. Two bands with molecular weights of 10 and 17 kDa are identified, are more abundant in transfected cells and correspond to two BOLA2 protein isoforms arising from different translation start sites.

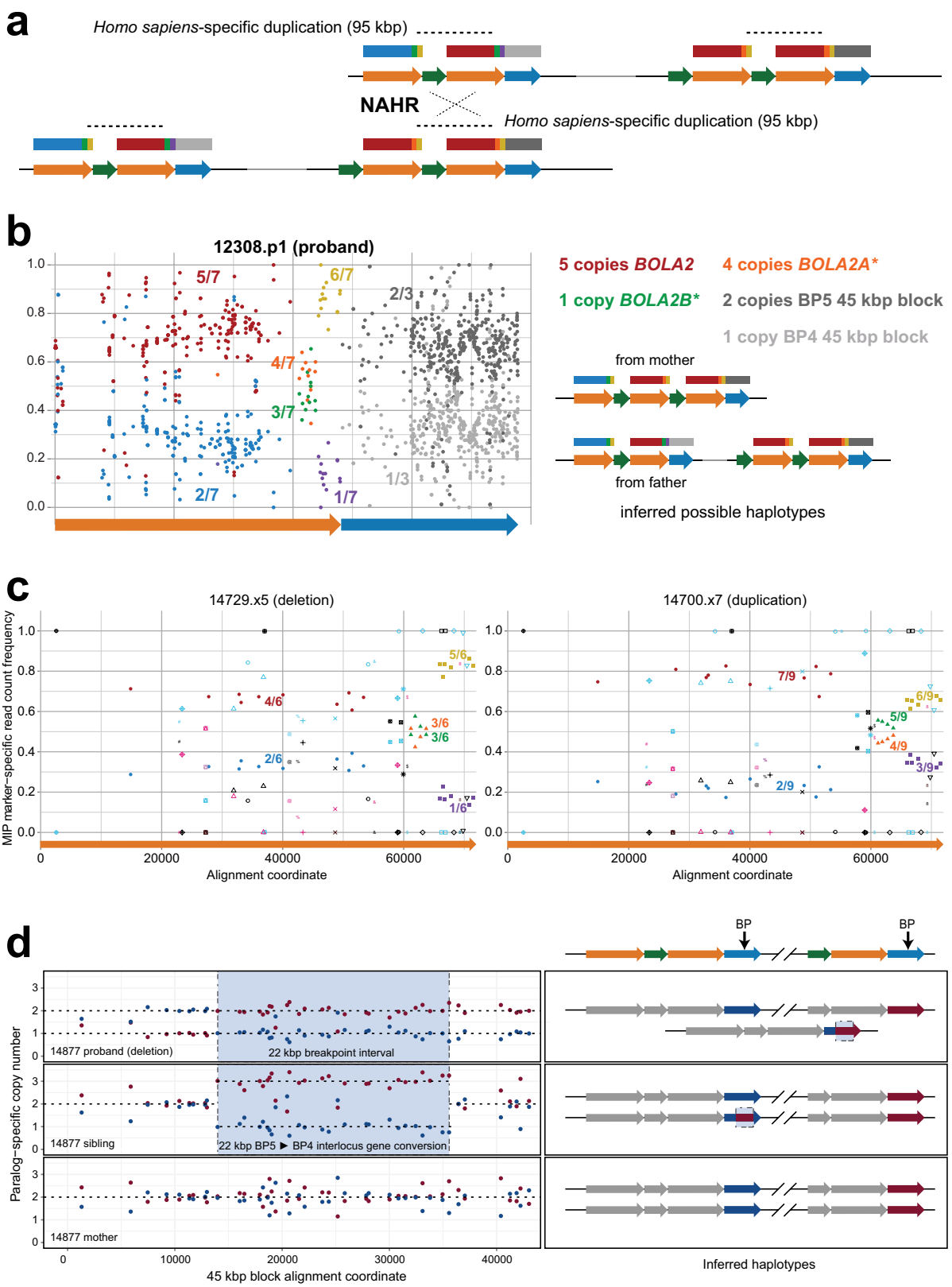

Extended Data Figure 10 | See next page for caption.

Extended Data Figure 10 | Chromosome 16p11.2 rearrangement breakpoint refinement. a, NAHR between directly oriented segmental duplications at BP4 and BP5. This unequal crossover results in chromosome 16p11.2 microdeletions and microduplications (Extended Data Fig. 5c). Coloured arrows and boxes correspond to duplication blocks and sectors within them are colour-coded as in Extended Data Fig. 7c. Unequal crossover could occur in eight distinct regions with regard to duplication block and sector boundaries. Three such regions are located within the ~95-kbp *H. sapiens*-specific duplication (dashed lines). Only unequal crossover events outside the *H. sapiens*-specific duplication produce recombinants which have a sector with non-uniform marker-specific copy number across its extent. **b**, Relative marker-specific read count frequencies (points) determined from WGS analysis for a microdeletion proband. Fractions indicate relative marker-specific copy numbers, as in Extended Data Fig. 7d, and diagrams adjacent to the plot show inferred haplotype structures for each chromosome 16 homologue for this individual. Although the data in the plot provide only diploid genotypes (and not resolved haplotypes), the haplotypes suggested here reflect this genotype information together with data from the parents (not shown) and the assumption (supported by our PSCN data) that haplotypes which have two *BOLA2A* copies and a single *BOLA2B* copy are the most common. Because marker-specific copy number is uniform across each sector, unequal crossover breakpoints must have occurred within the *H. sapiens*-specific duplication. **c**, Breakpoint refinement based on MIP PSCN marker data. Plots show relative marker-specific read count frequencies (points) determined using MIPs for a typical microdeletion patient (left) and a typical microduplication patient (right). Shapes and colour code designate different markers, and fractions indicate relative marker-specific copy numbers (as in Extended Data Fig. 7). Because marker-specific copy number is uniform across each sector for both individuals, in both cases, unequal crossover breakpoints must have occurred within the *H. sapiens*-specific duplication. **d**, Data from an atypical patient where the breakpoints are inferred to map outside the *H. sapiens*-specific segmental duplication. The plots show paralogue-specific copy number for a chromosome 16p11.2 microdeletion proband, his sibling and his mother over a 45-kbp duplication block shared between BP4 and BP5. Paralogue-specific copy number was estimated using a MIP assay targeting 54 informative markers over this region, with data from 43 markers fixed among haplotypes H1–H4 shown (points). Dashed lines indicate calls inferred using an automated caller, which were also confirmed by visual inspection. Adjacent schematics indicate the inferred haplotypes for each individual on the basis of these data, with approximate breakpoint locations shown (arrows). The results demarcate the location of the unequal crossover interval on the basis of the reciprocal copy number transition between the BP5 (red) and BP4 (blue) 45-kbp block segmental duplications. In this case, the breakpoints clearly map to a 22-kbp region outside the typical hotspot. Analysis of the sibling suggests that this region was the site of an interlocus gene conversion event from BP5 to BP4, and data from the mother imply that chromosomes having this event were present in the paternal germline. DNA from the father was not available for testing.